Tellus SERIES B CHEMICAL AND PHYSICAL METEOROLOGY
PUBLISHED BY THE INTERNATIONAL METEOROLOGICAL INSTITUTE IN STOCKHOLM

Tellus (2008), 60B, 525–536

TELLUS

An idealized model of the one-dimensional carbon dioxide rectifier effect

By VINCENT E. LARSON* and HANS VOLKMER, *Department of Mathematical Sciences, University of Wisconsin – Milwaukee, Milwaukee, WI, USA*

(Manuscript received 22 October 2007; in final form 3 June 2008)

ABSTRACT

The net flux of carbon dioxide (CO_2) from the land surface into the atmospheric boundary layer has a diurnal cycle. Drawdown of CO_2 occurs during daytime photosynthesis, and return of CO_2 to the atmosphere occurs during night. Even when the net diurnal-average surface *flux* vanishes, the diurnal-average *profile* of atmospheric CO_2 mixing ratio is usually not vertically uniform. This is because of the diurnal rectifier effect, by which atmospheric vertical transport and the surface flux conspire to produce a surplus of CO_2 near the ground and a deficit aloft.

This paper constructs an idealized, 1-D, eddy-diffusivity model of the rectifier effect and provides an analytic series solution. When non-dimensionalized, the intensity of the rectifier effect is related solely to a single 'rectifier parameter'. Given this model's governing equation and boundary conditions, we prove that the existence of the rectifier effect is related to the correlation of CO_2 gradient and transport, and also to the day–night symmetry of transport.

The rectifier-induced near-surface CO_2 surplus ought to be included in inverse calculations that use near-surface CO_2 mixing ratio to infer land–surface sources and sinks of carbon. Such inverse modeling is facilitated by our model's simplicity. To illustrate, we use a 1-D inverse calculation to infer the amplitude of diurnal CO_2 surface flux.

1. Introduction: What is the rectifier effect?

The flux of carbon dioxide (CO_2) from the land surface to the atmosphere undergoes a diurnal cycle. During the day, photosynthesis occurs, leading to a net flux of CO_2 from the atmosphere to biomass. During the night, respiration of CO_2 occurs; respiration is a result of plant decomposition, for instance, and leads to emission of CO_2 to the atmosphere. This oscillating diurnal flux of CO_2 is more or less symmetric between day and night, and is roughly sinusoidal (Baker et al., 2003; Davis et al., 2003). An observed example from Davis et al. (2003) is shown in Fig. 1.

In contrast to the flux, the near-surface time series of CO_2 *mixing ratio* is often asymmetric. In particular, the mixing ratio often peaks sharply in the wee hours of the morning and exhibits a long period of moderately low values during the day. Rather than being symmetric, the near-surface mixing ratio time series is 'rectified' (Heimann et al., 1986; Keeling et al., 1989; Denning et al., 1995, 1996a,b, 1999). Observations of this from Yi et al. (2000) are presented in Fig. 2. In these observations, the time series of CO_2 mixing ratio at 11 m is not quasi-sinusoidal, but rather has a truncated sinusoidal appearance reminiscent of a rectified electrical alternating current.

Given the quasi-symmetry of the time series of CO_2 flux, the observed asymmetry of the time series of mixing ratio may at first seem paradoxical. This diurnal rectifier effect results from differences in turbulent mixing between night and day (Denning et al., 1996b). During the night, the atmospheric boundary layer is often stable and shallow, causing CO_2 mixing ratio to build up strongly in a thin layer near the surface. During the day, the boundary layer is often convective and deep, causing the deficit in mixing ratio to be diluted over a large vertical extent. The resulting time-average vertical profile of CO_2 has an excess of CO_2 near the ground and a deficit aloft. This is illustrated by the observations in Fig. 2, which show that at night CO_2 decreases sharply with increasing altitude, and that the time-average mixing ratio at 11 m is larger than at 396 m.

The model that we develop is 1-D in the vertical coordinate, and it allows horizontal advective transports only to be specified, not calculated interactively. Our model is most immediately applicable in places with local horizontal homogeneity and a diurnal rectifier effect. In nature there also exists a similar *seasonal* rectifier effect, with winter playing the role of night and the summer growing season playing the role of day. In fact, the seasonal rectifier is thought to be larger than the diurnal rectifier (Denning et al., 1996b). On long time scales, air parcels

*Corresponding author.
e-mail: vlarson@uwm.edu
DOI: 10.1111/j.1600-0889.2008.00368.x

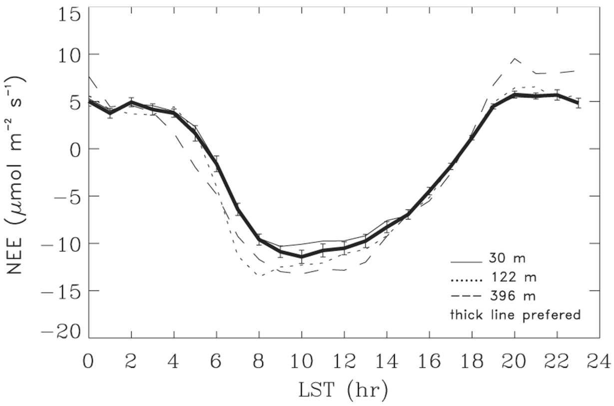

Fig. 1. Net ecosystem-atmosphere exchange (NEE) versus Local Standard Time (LST). NEE is the net CO_2 flux near the surface and corresponds to $-\tilde{K}\partial\tilde{c}/\partial\tilde{z}|_{\tilde{z}=0}$ in our model. The data show a diurnal composite for June–August 1997. The curves are derived mostly from eddy-covariance flux measurements on the WLEF tall tower in northern Wisconsin at altitudes of 30, 122, and 396 m. The thick solid line shows a blend of measurements from all three altitudes. The CO_2 surface flux time series has a quasi-sinusoidal shape, as assumed in our model's lower boundary condition (2). Reproduced from fig. 3 of Davis et al. (2003); copyright 2003 Blackwell Publishing.

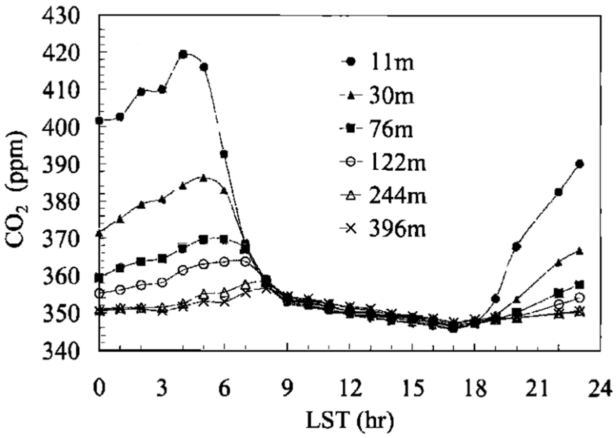

Fig. 2. Diurnal composite time series of CO_2 mixing ratio at various altitudes as measured at the WLEF tall tower in northern Wisconsin in July 1997. CO_2 is measured in parts per million, and time is plotted in Local Standard Time (LST). Note that near the ground (11 m), the time series appears similar in shape to a rectified electrical current, with a sharp peak of CO_2 during the night and a broad minimum during the day. Aloft (396 m), the diurnal cycle is much weaker and less asymmetric. Collectively, these time series indicate a diurnal-average profile that is non-uniform in the vertical, with a surplus of CO_2 near ground and a deficit aloft. Reproduced by permission of American Geophysical Union from fig. 1(a) of Yi et al. (2000); copyright 2000 American Geophysical Union.

can be advected horizontally from remote regions with disparate conditions and CO_2 mixing ratios. Because our model is 1-D, it applies to such rectifier effects only if the horizontal advective fluxes have a small net mean and little correlation with the vertical transport or vertical gradient of CO_2 (Yi et al., 2000; Davis et al., 2003; Chen et al., 2004). This paper will not discuss CO_2 effects that arise from horizontal transports such as the Hadley circulation and that are also sometimes denoted rectifier effects (Chen et al., 2004).

This near-surface vertical gradient of CO_2 contributes in turn to the observed Arctic-to-Antarctic CO_2 gradient near the surface. This is because the large land masses in the Northern Hemisphere have a stronger near-surface vertical gradient of CO_2 than do more southerly locations (Denning et al., 1995). Therefore, the Arctic-to-Antarctic CO_2 gradient is in part a secondary effect of the (vertical) diurnal and seasonal rectifier effects discussed above. However, this paper will restrict the term 'rectifier effect' to denote both the truncated sinusoidal near-surface time series, and the associated surplus near-surface CO_2 and deficit aloft in the time-average vertical profile. Both of these result from the covariance of vertical transport and surface flux of CO_2.

The rectifier effect is important in part because of its effect on inverse model calculations. Inverse models typically use measurements of CO_2 *mixing ratio* near the land or ocean surface and infer CO_2 *flux* at the surface. The surface flux, in turn, tells us about sources or sinks of CO_2 within the biosphere or ocean. In contrast to the highly localized fluxes yielded by direct measurement, inverse modeling yields average surface fluxes over broad areas, which is sometimes desirable. In the past, inverse modeling has been used primarily to derive CO_2 fluxes over continental-scale areas and monthly time scales, given near-surface observations of CO_2 mixing ratio at locations far from land (e.g. Gurney et al., 2002, 2003). However, there has also been interest in inverse calculations over land at subcontinental scales (Bakwin et al., 2004; Peylin et al., 2005) and diurnal or subdiurnal time scales (e.g. Law et al., 2004; Braswell et al., 2005).

The rectifier effect influences inverse calculations in part because it increases the time-averaged CO_2 mixing ratio near the surface. If this increase is not taken into account in a forward model, it may lead to an overestimate of a CO_2 source or an underestimate of a sink (Denning et al., 1995, 1996a; Gurney et al., 2002, 2003; Stephens et al., 2007). However, modeling the rectifier effect is difficult because it requires modeling small-scale vertical turbulent transport, particularly within the atmospheric boundary layer.

The 1-D rectifier effect has been observed and numerically simulated in prior works (Chen et al., 2004; Yi et al., 2004). The present paper develops an analytic model of it. Our primary goal is better conceptual understanding of the physics of the rectifier effect. However, the model may also be useful for inexpensive, approximate calculations, particularly analyses of tall-tower measurements of CO_2 mixing ratio that are used to invert diurnally varying sources and sinks at the surface. Inverse calculations may be facilitated by the fact that our model solutions depend only on a single non-dimensional parameter. Forward calculations may benefit from the fact that this single parameter can be used to prescribe the strength of the rectifier effect.

The structure of this paper is as follows. The model equation and boundary conditions are introduced in Section 2. A general analysis of when these equations yield rectified solutions is presented in Sections 3 and 4. An analytic series solution is presented and plotted in Section 5. An application of the model is illustrated with an inverse calculation in Section 6. Conclusions are listed in Section 7.

2. Model set-up

The geometry of the problem is assumed to be a horizontally uniform layer extending from the ground up to an infinite altitude. Therefore the problem is spatially 1-D in the vertical coordinate. We will use a tilde to denote variables having units and use no tilde for dimensionless variables. In contrast, for *constants or parameters*, no tilde will be used, regardless of whether they are dimensional or dimensionless.

We assume that turbulent transport is adequately modeled by an eddy diffusivity, $\tilde{K}$. Therefore, the atmospheric evolution of CO_2 is described by a diffusion equation for CO_2 mixing ratio. We will work in the *perturbation* mixing ratio, $\tilde{c}(\tilde{z},\tilde{t})$, from a reference value, $\tilde{c}_{\mathrm{ref}}$. We choose $\tilde{c}_{\mathrm{ref}}$ to equal the average of $\tilde{c}(\tilde{z},\tilde{t})$ over time $\tilde{t}$ *and* altitude $\tilde{z}$ that would occur if there were no source. The diffusion equation is:

$$\frac{\partial \tilde{c}(\tilde{z},\tilde{t})}{\partial \tilde{t}} = \frac{\partial}{\partial \tilde{z}}\left[\tilde{K}(\tilde{z},\tilde{t})\frac{\partial \tilde{c}(\tilde{z},\tilde{t})}{\partial \tilde{z}}\right] + \tilde{S}(\tilde{t}). \tag{1}$$

Here $\tilde{S}$ is an internal atmospheric source of CO_2 that we allow to vary in time but not in the vertical direction. Although CO_2 does not have a significant chemical source in the atmosphere, $\tilde{S}$ may crudely represent specified, column-averaged horizontal advection of CO_2.

At the lower boundary ($\tilde{z} = 0$) we impose a diurnal, sinusoidal flux of carbon because observed fluxes are often quasi-sinusoidal (e.g. Baker et al., 2003):

$$-\tilde{K}\left.\frac{\partial \tilde{c}}{\partial \tilde{z}}\right|_{\tilde{z}=0} = F_0\cos(\omega_0\tilde{t}). \tag{2}$$

Here $\omega_0 = 2\pi/(24\,\mathrm{h})$ is the angular frequency corresponding to one day, and F_0 is the maximum surface flux, with units of mixing ratio times velocity. We interpret $\tilde{t} = 0$ as midnight local time.

At the upper boundary ($\tilde{z} \to \infty$), we impose a CO_2 flux of zero:

$$-\tilde{K}(\tilde{z},\tilde{t})\left.\frac{\partial \tilde{c}(\tilde{z},\tilde{t})}{\partial \tilde{z}}\right|_{\tilde{z}=\infty} = 0. \tag{3}$$

We place the upper boundary at infinity in order to simplify the analytic solutions. However, the main variation in CO_2 occurs near the lower boundary, specifically, within the atmospheric boundary layer, which over land tends to be shallow at night [O($\sim$100 m)] and deeper during the day [O($\sim$1 km)] (e.g., fig. 1.7 of Stull, 1988; Yi et al., 2001).

We do not attempt to solve an initial value problem. Therefore we do not impose any initial condition. Instead, we assume periodic forcing and seek periodic solutions in time.

Now we non-dimensionalize the diffusion equation and boundary conditions. We choose a diffusivity scale $K_0 \approx 100$ to 1000 $\mathrm{m^2\,s^{-1}}$, a length scale $H = (2K_0/\omega_0)^{1/2} \approx 2$–5 km, a time scale $1/\omega_0$ equal to radians per day, and a CO_2 mixing ratio of

$$c_0 = F_0/(2\omega_0 K_0)^{1/2}. \tag{4}$$

Then the equation and boundary conditions become

$$\frac{\partial c(z,t)}{\partial t} = \frac{\partial}{\partial z}\left[\frac{K(z,t)}{2}\frac{\partial c(z,t)}{\partial z}\right] + S(t), \tag{5}$$

$$-\frac{K(z,t)}{2}\left.\frac{\partial c(z,t)}{\partial z}\right|_{z=0} = \cos(t), \tag{6}$$

and

$$-\frac{K(z,t)}{2}\left.\frac{\partial c(z,t)}{\partial z}\right|_{z=\infty} = 0, \tag{7}$$

where

$$c = (\tilde{c} - \tilde{c}_{\mathrm{ref}})/c_0, \tag{8}$$

and $K = \tilde{K}/K_0, t = \omega_0\tilde{t}, z = \tilde{z}/H$ and $S = \tilde{S}/(\omega_0 c_0)$. The choice of length scale introduces factors of 2 into the equation and boundary conditions but simplifies the solutions below.

3. When is the time-averaged profile of CO_2 uniform with altitude?

Prior works have noted that the rectifier effect stems from a non-zero temporal correlation between the surface flux of CO_2 and atmospheric vertical transport (Denning et al., 1996b; Heimann et al., 1986; Keeling et al., 1989; Stephens et al., 2000). Although we have not found a proof of this relationship, we now prove a somewhat related link between the concentration/transport covariance and the shape of the time-average CO_2 profile. In this section, we assume that the solution is time-periodic and that the time-averaged internal source of CO_2 vanishes, that is, that $\overline{S}^t = 0$.

We investigate the conditions under which the time average of CO_2 is uniform in the vertical, which corresponds to $\overline{c(z,t)}^t = 0$ at all altitudes. That is, we ask, When is

$$\overline{c(z,t)}^t \equiv \frac{1}{2\pi}\int_{-\pi}^{\pi} c(z,t)\mathrm{d}t = 0\ ? \tag{9}$$

Such a uniform profile is associated with an un-rectified solution.

First we average the left-hand side of the diffusion eq. (5) over one time period. Regardless of whether or not $\overline{c(z,t)}^t = 0$, if we assume periodic solutions with period 2π, then

$$\overline{\frac{\partial c}{\partial t}}^t = \frac{c(z,t=2\pi) - c(z,t=0)}{2\pi} = 0. \tag{10}$$

That is, CO_2 does not build up over time. This can be true only if the right-hand side of eq. (5) is zero:

$$\frac{\partial}{\partial z}\left(\overline{\frac{K}{2}\frac{\partial c}{\partial z}}^{t}\right) = 0. \tag{11}$$

(Recall that we have set $\overline{S}^t = 0$.) This implies that

$$\overline{K\frac{\partial c}{\partial z}}^{t} = \text{Constant} = 0, \tag{12}$$

at all altitudes, where we conclude that Constant = 0 because the upper boundary condition (7) imposes zero flux at the top boundary. The result (12) depends only on the assumptions of 1-D transport (5), periodicity, zero source $S(t)$, and zero flux at the upper boundary (7). The result holds true for both rectified and unrectified cases.

If we distinguish the two cases, however, we can go further. If the diurnally averaged flux is zero (eq. 12), then the daytime flux must be equal in magnitude but opposite in sign to the nighttime flux:

$$\overline{K\frac{\partial c}{\partial z}}^{\text{Day}} = -\overline{K\frac{\partial c}{\partial z}}^{\text{Night}}. \tag{13}$$

If the transport, here modeled by K (>0), is greater during the day than during the night, then $\partial c/\partial z$ must be smaller in magnitude during day than during night, which suggests a non-uniform (rectified) profile.

We can formalize this line of argument as follows. Applying Reynolds rules of averaging (Stull, 1988), we find

$$\overline{K}^t\,\overline{\frac{\partial c}{\partial z}}^{t} + \overline{K'\frac{\partial c'}{\partial z}}^{t} = 0, \tag{14}$$

where a prime denotes a deviation from the time average. Now suppose that $\overline{c(z,t)}^t = 0$ at all altitudes, as for an unrectified case, so that

$$\overline{\frac{\partial c}{\partial z}}^{t} = \frac{\partial \overline{c}^t}{\partial z} = 0. \tag{15}$$

Then the term $\overline{K}^t\ \overline{\partial c/\partial z}^t$ is zero and

$$\overline{K'\frac{\partial c'}{\partial z}}^{t} = 0. \tag{16}$$

Therefore, if $\overline{c(z,t)}^t = 0$ (i.e. the CO_2 profile is uniform as for an unrectified case), then in this model there is no temporal covariance between perturbation K (i.e. transport) and perturbation $\partial c/\partial z$ (i.e. concentration gradient).

Likewise, if $c(z, t)$ vanishes at the upper boundary and if $\overline{K}^t \neq 0$, then one may prove the converse: if $\overline{K'\partial c'/\partial z}^t = 0$, then $\overline{c}^t = 0$. The proof proceeds by following the steps used to derive eqs (9)–(14), setting $\overline{K'\partial c'/\partial z}^t = 0$ in eq. (14) by assumption, noting that $\partial \overline{c}^t/\partial z = 0$ if $\overline{K}^t > 0$, using vertical integration to show that $\overline{c}^t$ is constant with respect to z, and finally using the fact that c is a perturbation from $\tilde{c}_{\text{ref}}$ to conclude that $\overline{c}^t = 0$.

4. When is the time series of CO_2 perturbation symmetric?

The previous section discussed *time-average profiles* of $c(z, t)$, and particularly the cause of vertically uniform time-average profiles. This section discusses periodic time *series* of $c(z, t)$, and the cause of equal but opposite values of $c(z, t)$ during day and night, as would occur in our model for an unrectified solution.

We prove that if $c(z, t)$ is a solution of the diffusion eq. (5) with boundary conditions (6) and (7), and if

$$K(z,t) = K(z, t+\pi) \quad S(t) = -S(t+\pi), \tag{17}$$

then $-c(z, t+\pi)$ is also a solution. Here an eddy diffusivity $K(z, t) = K(z, t+\pi)$ means simply that K is periodic with a period of one-half day. In other words, K, and hence the transport, behaves the same during the day as during the night, as would be the case in an unrectified situation. The source $S(t)$ is assumed to have day–night antisymmetry and zero diurnal mean. The proof simply involves letting $t \to t+\pi$ in eqs (5), (6) and (7). By inspection, one sees that $-c(z, t+\pi)$ satisfies the eq. (5) and boundary conditions (6-7). The proof follows in part because the surface flux, $f_s(t) = \cos(t)$, satisfies $f_s(t) = -f_s(t+\pi)$.

If both $c(z, t)$ and $-c(z, t+\pi)$ are solutions, then, because of linearity, there also exists the solution

$$c_a(z,t) = \frac{c(z,t) - c(z,t+\pi)}{2}, \tag{18}$$

which also satisfies the boundary conditions (6)–(7). If $c_a(z, t)$ has a period of 2π, then, it is straightforward to show, by integration of (18) over a period, that

$$\overline{c_a(z,t)}^t = 0. \tag{19}$$

Inspection of (18) reveals that $c_a(z, t)$ obeys the following periodic antisymmetry:

$$c_a(z,t) = -c_a(z, t+\pi). \tag{20}$$

Examples of such periodic, antisymmetric functions are the sinusoids $c_a(z, t) = f(z)\sin(nt+\phi)$ or $f(z)\cos(nt+\phi)$, where $n = \pm 1, \pm 3, \ldots$ and ϕ is an arbitrary phase. In such solutions, the perturbation mixing ratio at one time is the opposite of what it is a half-day earlier or later. For instance, a reduction of CO_2 during the day matches an equal but opposite increase in CO_2 during the night.

Perhaps of more interest is to demonstrate the converse, that is, that if $K(z, t) \neq K(z, t+\pi)$, then $c_a(z, t) = -c_a(z, t+\pi)$ cannot be a solution. In other words, if the transport differs between night and day, then the CO_2 time evolution must be asymmetric (e.g. rectified) and not, for instance, sinusoidal (unrectified). We now prove this under plausible conditions given below. We proceed by proving the logical equivalent, the contrapositive: If $c_a(z, t)$ is a solution of the diffusion eq. (5), the lower boundary condition (6), and the upper boundary condition (7), and assuming $S(t) = -S(t+\pi)$, then $K(z, t) = K(z, t+\pi)$. The proof is as follows. If $c_a(z, t)$ solves (5), (6) and (7), then, by letting $t \to t + \pi$, it can be shown that $c_a(z, t)$ solves the same eqs (5), (6) and (7) but with $K(z, t)$ replaced everywhere by $K(z, t + \pi)$. If we compare the original lower boundary condition (6) that includes $K(z, t)$, with the version of (6) written in terms of $K(z, t + \pi)$, i.e.

$$-\frac{K(z, t+\pi)}{2} \frac{\partial c_a(z, t)}{\partial z}\bigg|_{z=0} = \cos(t), \tag{21}$$

then we can directly conclude that $K(0, t) = K(0, t + \pi)$ whenever $\partial c_a(0, t)/\partial z \neq 0$. In the special case that K is independent of z, then the result is proved. On the other hand, if K depends on z, then we need to subtract two versions of the diffusion eq. (5) for $c_a(z, t)$, one containing $K(z, t)$ and the other containing $K(z, t + \pi)$. The time tendency term on the left-hand side vanishes. We find

$$\frac{\partial}{\partial z}\left\{[K(z, t) - K(z, t+\pi)] \frac{\partial c_a(z, t)}{\partial z}\right\} = 0. \tag{22}$$

Then we integrate vertically from z to ∞ and use the upper boundary condition (7) to show that

$$[K(z, t) - K(z, t+\pi)] \frac{\partial c_a(z, t)}{\partial z} = 0. \tag{23}$$

Therefore, wherever and whenever $\partial c_a/\partial z$ is non-zero, $K(z, t) = K(z, t + \pi)$. This concludes the proof.

5. Model solutions

5.1. A general, periodic series solution

For the remainder of this paper, we will assume that the eddy diffusivity, K, is independent of altitude. Clearly this is a crude approximation for the earth's atmosphere. However, the assumption permits simple analytic solutions that are qualitatively realistic. We prescribe a sinusoidal diurnal cycle in K:

$$K = 1 - \alpha \cos(t). \tag{24}$$

Here, α is a parameter that lies within the range $0 \leq \alpha < 1$. Given the model (24), K is greater during the day, when the ground is heated and turbulent convection is more common, and lesser at night, when the atmosphere is often stably stratified. In this case, K does not have the day–night symmetry (17), and hence $c(z, t)$ is not expected to have equal but opposite values during the day as during night.

The formulation (24) permits a large diurnal variation in K if α is chosen to be large. For instance, if $\alpha = 0.95$, then during the day $K(= 1.95)$ is 39 times larger than it is at night ($K = 0.05$). Still larger variation in K requires larger values of α, which leads to slow convergence. Because arbitrarily large K cannot be used, this model, as typical for eddy diffusivity models, cannot produce the highly well-mixed profiles that are sometimes seen in observations.

The formulation (24) restricts the phase of K to be opposite of the phase of the surface flux (6). For instance, at noon transport (K) maximizes, and the surface flux is most negative. On the contrary, in many cases in nature, the transport may peak later in the afternoon. The effect of this offset in phase cannot be studied with our model as presented.

In the remainder of this section (Section 5), we will set the source $S(t) = 0$, for simplicity. However, if one wishes to account for non-zero S, one simply needs to add to the solution below a particular solution, call it c_p, that obeys homogeneous boundary conditions,

$$c_p(t) = \int_{-\infty}^{t} S(t')\mathrm{d}t', \tag{25}$$

where we assume that the source is such that the integral is finite.

We seek a time-periodic solution to the diffusion eq. (5) with boundary conditions (6) and (7). We use separation of variables for z and t (e.g. chapter 13 of Boas, 1983). That is, we seek solutions of a special form in which the variables z and t appear in separate functions, which we denote Z and T. Since the equation for c is linear, such solutions may be summed:

$$c(z, t) = \sum_m Z_m(z) T_m(t). \tag{26}$$

After standard manipulations, we find the following series solution to (5):

$$c(z, t) = \sum_{m=1}^{\infty} \frac{A_m}{\sqrt{m}} e^{-\sqrt{m}z} [\cos\psi - \sin\psi], \tag{27}$$

where

$$\psi \equiv \sqrt{m}z - mt + m\alpha \sin(t). \tag{28}$$

We have retained only the solution that decays as $z \to \infty$ in order to satisfy the upper boundary condition (7).

We choose the A_m coefficients such that they satisfy the lower boundary condition (6), which sets the surface flux to a simple cosine. By substituting (27) for $c(z, t)$ and (24) for K into the flux at the lower boundary, we find that

$$-\frac{K}{2} \frac{\partial c}{\partial z}\bigg|_{z=0} = [1 - \alpha\cos(t)] \sum_{m=1}^{\infty} A_m \cos\{m[t - \alpha\sin(t)]\}. \tag{29}$$

To simplify, we introduce a new variable

$$\tau = t - \alpha \sin t. \tag{30}$$

The variable τ may be interpreted as a distorted time coordinate. Note that $\mathrm{d}\tau/\mathrm{d}t = K(t) = 1 - \alpha \cos(t)$. Thus, time intervals in τ are shorter relative to those in t when K is small (i.e. during nighttime); time intervals in τ are longer relative to those in t when K is large (i.e. during daytime). When written in terms of τ, the diffusion eq. (5) with $K = K(t)$ and $S = 0$ has a constant diffusivity with magnitude 1/2. This implies that, viewed in the distorted time coordinate, CO_2 diffuses with a constant eddy diffusivity. Therefore, $c(z, \tau)$ becomes a series of simple sinusoids in τ (see eqs 27, 28 and 30).

Combining the lower boundary condition (6), the flux at the lower boundary (29), and the new time coordinate (30), we find

$$\frac{\cos t}{1-\alpha\cos t} = \sum_{m=1}^{\infty} A_m \cos(m\tau). \tag{31}$$

The coefficients A_m may be regarded as Fourier coefficients in τ that can be obtained in the usual manner (chapter 7 of Boas, 1983):

$$\begin{aligned} A_m &= \frac{2}{\pi}\int_0^{\pi} \frac{\cos t}{1-\alpha\cos t}\cos(m\tau)\,\mathrm{d}\tau \\ &= \frac{2}{\pi}\int_0^{\pi} \cos t\cos[m(t-\alpha\sin t)]\,\mathrm{d}t \\ &= \frac{2}{\alpha} J_m(m\alpha). \end{aligned} \tag{32}$$

Here J_m is the mth Bessel function. The second integral can be evaluated by using the cosine product formula, an integral expression for Bessel functions (eq. 3.719 of Gradshteyn and Ryzhik, 1980), and a recurrence relationship between Bessel functions (eq. 9.1.27 of Abramowitz and Stegun, 1965).

The series (27) is most useful for small α, because then only a few terms need to be kept. However, with the aid of a computer, the solution may easily be obtained for α as large as 0.95 by retaining 50 terms. For larger values of α, convergence of the series is very slow.

The time-average concentration is:

$$\overline{c(z,t)}^{t} = \sum_{m=1}^{\infty} \frac{A_m}{\sqrt{m}} J_m(m\alpha) e^{-\sqrt{m}z}[\cos(\sqrt{m}z) - \sin(\sqrt{m}z)]. \tag{33}$$

By substituting (32) into (33), we see that at the surface ($z = 0$), (33) reduces to

$$\overline{c(z=0,t)}^{t} = \frac{2}{\alpha}\sum_{m=1}^{\infty} \frac{[J_m(m\alpha)]^2}{\sqrt{m}}. \tag{34}$$

By Taylor expanding the Bessel functions in polynomials about $\alpha = 0$ (eq. 9.1.10 Abramowitz and Stegun, 1965), we find the approximate form

$$\overline{c(z=0,t)}^{t} \approx 0.5\alpha + 0.229\alpha^3 + 0.143\alpha^5. \tag{35}$$

Recall that $c(z, t)$ is the non-dimensionalized, perturbation mixing ratio: $c(z,t) = (\tilde{c}(\tilde{z},\tilde{t}) - \tilde{c}_{\mathrm{ref}})/c_0$. In dimensional form, eq. (35) becomes

$$\overline{\tilde{c}(\tilde{z}=0,\tilde{t})}^{\tilde{t}} \approx \tilde{c}_{\mathrm{ref}} + \frac{F_0}{\sqrt{2\omega_0 K_0}}\left(0.5\alpha + 0.229\alpha^3 + 0.143\alpha^5\right). \tag{36}$$

Equation (35), while accurate for small α, is an underestimate when α approaches 1. Alternatively, we may expand (34) in a series of Chebyshev polynomials and collect powers (e.g. section 13.4 of Arfken, 1985):

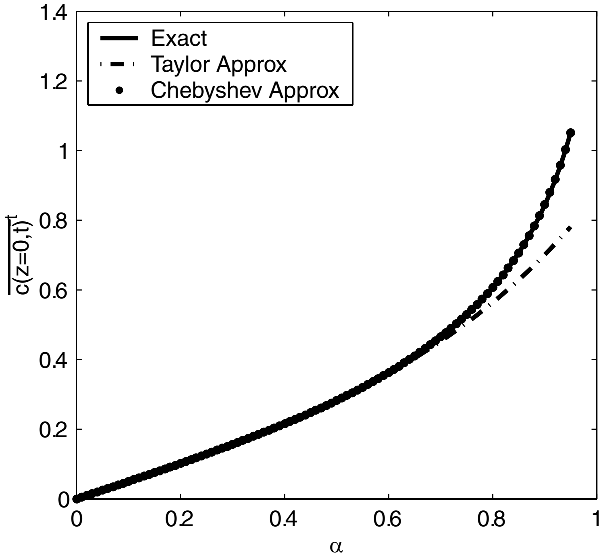

Fig. 3. Surface CO_2 mixing ratio versus the rectifier parameter α, plotted over the range $0 < \alpha \le 0.95$. The solid line depicts the first 50 terms of the exact normalized perturbation surface CO_2 mixing ratio $\overline{c}^t = (\overline{\tilde{c}}^t - \tilde{c}_{\mathrm{ref}})/c_0$ (eq. 34). The dashed line depicts the Taylor series approximation (eq. 35), which is accurate for $0 \le \alpha \lesssim 0.7$. The dotted line denotes the Chebyshev polynomial approximation (eq. 37), which is accurate over the full plotted range.

$$\begin{aligned} \overline{c(z=0,t)}^{t} \approx{}& 0.500\,\alpha + 0.067\,\alpha^2 - 1.232\,\alpha^3 + 11.586\,\alpha^4 \\ &- 42.368\,\alpha^5 + 78.302\,\alpha^6 - 70.654\,\alpha^7 + 25.174\,\alpha^8. \end{aligned} \tag{37}$$

For all values of α between $0 < \alpha \le 0.95$, approximation (37) remains within 0.004 of (34). In Fig. 3, we plot the exact formula (34) but with only 50 terms retained, the Taylor expansion (35) and the Chebyshev expansion (37). The Taylor expansion is inaccurate for large α, but the Chebyshev approximation is nearly indistinguishable from the exact formula over the entire range plotted.

These formulas indicate how the rectifier parameter α affects the average surplus surface CO_2 mixing ratio associated with the rectifier effect. The surplus mixing ratio becomes more sensitive to the value α for larger values of α.

5.2. *A simple model with a closed-form asymmetric solution*

If we desire to find an exact solution that has only one term, then we may modify the lower boundary condition as follows:

$$-\frac{K}{2}\frac{\partial c}{\partial z}\bigg|_{z=0} = [1-\alpha\cos(t)]\cos[t-\alpha\sin(t)]. \tag{38}$$

This boundary condition is more complex and less realistic than the boundary condition (6), but it leads to a simple solution.

[Since this boundary condition does not have the symmetry of $\cos(t)$ in general, it does not permit the symmetry arguments of the previous section.] Again using separation of variables, we find

$$c(z,t) = e^{-z}\left\{\cos\left[z - t + \alpha \sin(t)\right] - \sin\left[z - t + \alpha \sin(t)\right]\right\}. \tag{39}$$

One can time-average this solution over a diurnal cycle to find an averaged CO_2 mixing ratio, $\overline{c(z,t)}^t$. One finds

$$\overline{c(z,t)}^t = J_1(\alpha)e^{-z}\left[\cos(z) - \sin(z)\right]. \tag{40}$$

For small α (eq. 9.1.10 Abramowitz and Stegun, 1965),

$$J_1(\alpha) \approx \frac{1}{2}\alpha. \tag{41}$$

5.3. *A special case: an antisymmetric solution*

The previous solutions permit $\alpha \neq 0$, in which case K does not obey the day–night symmetry (17), and hence $\overline{c(z,t)}^t \neq 0$. In contrast, when $\alpha = 0$, then $K = 1$ and $c(z, t)$ becomes antisymmetric with $\overline{c(z,t)}^t = 0$.

Here, for purposes of comparison with the previous solutions, we set $\alpha = 0$ and $K = 1$ in the governing eq. (5) and boundary conditions (6) and (7). We find via separation of variables, for example, that a time-periodic solution is

$$c(z,t) = e^{-z}\left[\cos(z - t) - \sin(z - t)\right]. \tag{42}$$

This is also the solution to which (40) reduces when $\alpha = 0$. Because K has the symmetry (17), the solution has the antisymmetry of $c_a(z, t)$ (20), as expected by our symmetry proof of Section 4. Furthermore, the diurnal average is

$$\overline{c(z,t)}^t = 0, \tag{43}$$

as expected by our proof of Section 3. The solution is unrectified.

5.4. *Plots of solutions*

By varying the rectifier parameter α, the series solution (27) allows us to compute solutions that range from perfectly symmetric and unrectified ($\alpha = 0$) to highly asymmetric and rectified (e.g. $\alpha = 0.95$). These two extremes are plotted, respectively, in the left- and right-hand columns of Fig. 4.

The top right-hand panel (rectified case) shows a sharp peak of CO_2 mixing ratio at night and a deeper layer during the day. The diurnal-mean profile of CO_2 in the top right-hand panel is rectified and looks qualitatively similar to fig. 3(a) of Yi et al. (2004).

The middle row plots the eddy diffusivity, the surface CO_2 mixing ratio and the surface CO_2 flux. The surface mixing ratio is symmetric with time in the unrectified case (middle left-hand panel) and asymmetric in the rectified case (middle right-hand panel) as expected from the symmetry proof of Section 4. The surface CO_2 flux in either case is prescribed to be a cosine and appears qualitatively similar to Fig. 1 above and to fig. 7 of Baker et al. (2003).

The bottom row shows the time series of CO_2 mixing ratio at various altitudes. The unrectified solutions are symmetric with time, as expected. The rectified solutions have features that agree qualitatively with the observations in Fig. 2. For instance, mixing ratios vary strongly with altitude at night, when the boundary layer is stratified, and the mixing ratios vary little with altitude during the day, when the boundary layer is better mixed (also see, e.g. fig. 10 of Chen et al., 2004). However, we note that the top right-hand panel does indicate that the modelled daytime profile of CO_2 is not perfectly well mixed, even when $\alpha = 0.95$. Instead, the model shows a slight increase of CO_2 with altitude during the day, because the eddy diffusivity always transports CO_2 downgradient and hence requires a positive vertical gradient in order to transport CO_2 toward the sink at the ground. This lack of well mixedness is an oft-noted shortcoming of eddy diffusivity models in general. Relatedly, the time series at different altitudes in the lower right-hand panel do not overlap during daytime (i.e. the profile is not well mixed), in contrast to the observations shown in Fig. 2.

6. Inverse modeling

The dimensionless model described above quantifies the strength of the rectifier effect in terms of a single dimensionless parameter, α. The simplicity of the model facilitates inverse modeling. In a typical CO_2 inverse model calculation, one measures the CO_2 mixing ratio in the atmosphere and infers the net flux of CO_2 into the atmosphere from the underlying land or ocean surface. The surface flux provides information about sources and sinks of CO_2 such as growth of biomass via photosynthesis. An advantage of using CO_2 mixing ratio to infer CO_2 flux is that it provides an estimate of the flux over a broader region than is possible using a single direct measurement of CO_2 flux.

To illustrate how the above model of the rectifier effect can simplify inverse calculations, we consider the 1-D problem of separately inferring the daytime and nighttime surface CO_2 fluxes. This might be useful because it begins to help separate the sink of CO_2 due to daytime photosynthesis from sources such as nighttime respiration.

As input data for our problem, suppose that we measure a continuous time series of CO_2 concentration measurements at the ground and at one higher altitude. Such measurements are taken at several research towers across the globe (Bakwin et al., 2004). The output of our inverse calculation is a complete but approximate solution of 1-D (vertical) CO_2 evolution and transport, including the amplitude of the diurnally varying flux, F_0 of eq. (2). The inferred flux represents a broad areal average, in contrast to a direct measurement of the flux.

For simplicity, we assume that the internal atmospheric ‘source’ of CO_2, $\tilde{S}$, is known. This ‘source’ could crudely represent horizontal advection of CO_2 into or out of the 1-D

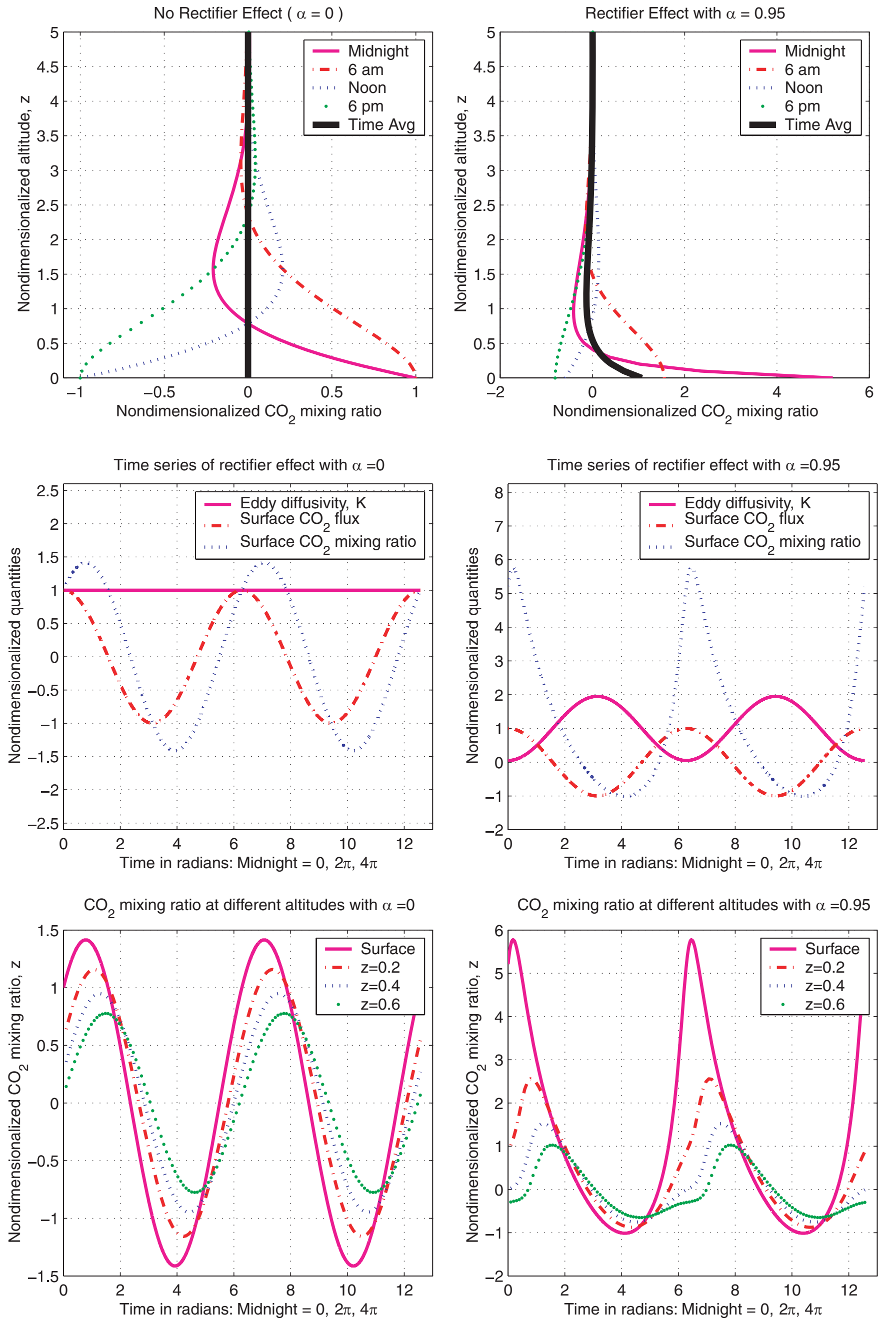

Fig. 4. Plots of the model solution for CO_2 mixing ratio (eq. 27), eddy diffusivity (eq. 24), and CO_2 flux at the surface (eq. 6). The left-hand column of panels has no rectification ($\alpha = 0$), and the right-hand column of panels has strong rectification ($\alpha = 0.95$). The top right-hand panel shows that the time-averaged rectified profile of CO_2 mixing ratio has an excess of CO_2 near the surface and a deficit aloft. The middle row shows that the time series of surface CO_2 mixing ratio when $\alpha = 0.95$ has a classic rectified shape (middle right-hand panel), with a sharp peak at night and a moderate minimum during the day; when $\alpha = 0$ (middle left-hand panel), the time series is sinusoidal. The bottom row of panels shows that with $\alpha = 0.95$, the CO_2 mixing ratio is stratified at night but more well-mixed during the day.

grid column of interest. The four input measurements are: the first and second Fourier cosine coefficients $\tilde{a}_1$ and $\tilde{a}_2$ of the CO_2 time series, and the mean at the surface, $\overline{\tilde{c}(\tilde{z}=0,\tilde{t})}^{\tilde{t}}$, and at some altitude aloft, $\overline{\tilde{c}(\tilde{z}=\tilde{z}_1,\tilde{t})}^{\tilde{t}}$. The four unknown parameters of the problem and the equations that define them are α (24), c_0 (4), F_0 (2) and $\tilde{c}_{\mathrm{ref}}$ (8).

The nth Fourier cosine coefficient ($n = 1, 2, 3, \ldots$) of the surface CO_2 mixing ratio, $\tilde{c}(\tilde{z}=0,\tilde{t})$, is given by

$$\tilde{a}_n = \frac{\omega_0}{\pi} \int_{-\pi/\omega_0}^{\pi/\omega_0} \cos(n\omega_0 \tilde{t})\, \tilde{c}(\tilde{z}=0,\tilde{t})\, \mathrm{d}\tilde{t}$$

$$= c_0 \sum_{m=1}^{\infty} \frac{A_m}{\sqrt{m}} \left[J_{m+n}(m\alpha) + J_{m-n}(m\alpha) \right]. \quad (44)$$

Both Fourier series theory and our rectifier solutions assume infinite, periodic time series. Such time series do not exist in real observational data. Therefore, to best match theory and data, it is advantageous either to select data from multiple similar days, or to condition the data by detrending and tapering (Stull, 1988, pp. 308–310), or both.

Once the input measurements have been made, then the inversion requires four steps:

(i) Given the ratio $\tilde{a}_2/\tilde{a}_1$, infer the rectifier parameter, α, using the following implicit equation for α:

$$\frac{\tilde{a}_2}{\tilde{a}_1} = \frac{\sum_{m=1}^{\infty} \frac{A_m}{\sqrt{m}} \left[J_{m+2}(m\alpha) + J_{m-2}(m\alpha) \right]}{\sum_{m=1}^{\infty} \frac{A_m}{\sqrt{m}} \left[J_{m+1}(m\alpha) + J_{m-1}(m\alpha) \right]}. \quad (45)$$

Recall that the coefficient A_m is a function of α alone and is given by eq. (32). Solving for α requires the use of a numerical root finder. However, this is a relatively easy task, since the value of $\tilde{a}_2/\tilde{a}_1$ uniquely specifies a value of α. Fig. 5 plots the functional relationship, which may be used to perform the inversion graphically.

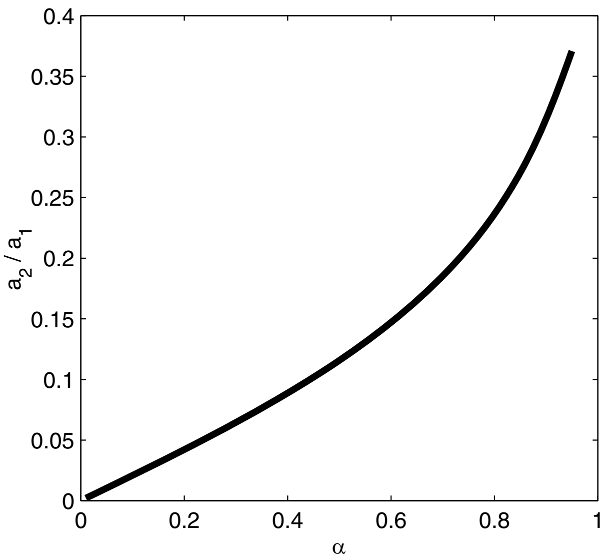

Fig. 5. The ratio of the second to first cosine Fourier components, $a_2/a_1 = \tilde{a}_2/\tilde{a}_1$, as a function of the rectifier parameter, α, plotted over the range $0 < \alpha \leq 0.95$. Because of the simple one-to-one relationship, if a_2/a_1 is calculated from an accurately measured time series of CO_2 mixing ratio, then α can be easily inferred.

(ii) Given $\tilde{a}_1$ (and α), calculate c_0 [$= F_0/(2\,\omega_0\,K_0)^{1/2}$] from eq. (44):

$$c_0 = \tilde{a}_1 \left\{ \sum_{m=1}^{\infty} \frac{A_m}{\sqrt{m}} \left[J_{m+1}(m\alpha) + J_{m-1}(m\alpha) \right] \right\}^{-1}. \quad (46)$$

This calculation is straightforward. With α and c_0 inferred, we already possess enough information to determine the surface mixing ratio surplus, $\overline{\tilde{c}(\tilde{z}=0,\tilde{t})}^{\tilde{t}} - \tilde{c}_{\mathrm{ref}}$ (see eq. 48 below).

(iii) Given the difference of average CO_2 mixing ratio at the surface and at altitude $\tilde{z}_1$, $\overline{\tilde{c}(\tilde{z}=0,\tilde{t})}^{\tilde{t}} - \overline{\tilde{c}(\tilde{z}=\tilde{z}_1,\tilde{t})}^{\tilde{t}}$, and given α and c_0 from steps (i) and (ii), then infer the scale height of CO_2 mixing, H, where $H \equiv (2K_0/\omega_0)^{1/2}$ (see Section 2). If K_0 is assumed to be unknown, then measurements of surface CO_2 mixing ratio alone are insufficient to determine H, and we need measurements of CO_2 mixing ratio aloft. This is because the same surface time series of CO_2 mixing ratio can correspond to a range of solutions. Some solutions have a strong surface flux of CO_2 (F_0) and eddy diffusivity K_0; this leads to transport of CO_2 over a deep layer (i.e. large H). Other solutions have a weak surface flux (F_0) and eddy diffusivity (K_0); this leads to variations over a shallow layer (i.e. small H). We infer H by numerically finding the roots of the following implicit equation for H, which is derived from eq. (33):

$$\frac{\overline{\tilde{c}(\tilde{z}=0,\tilde{t})}^{\tilde{t}} - \overline{\tilde{c}(\tilde{z}=\tilde{z}_1,\tilde{t})}^{\tilde{t}}}{c_0} = \sum_{m=1}^{\infty} \frac{A_m}{\sqrt{m}} J_m(m\alpha) \left\{ 1 - e^{-\sqrt{m}\tilde{z}_1/H} \left[\cos\left(\frac{\sqrt{m}\tilde{z}_1}{H}\right) - \sin\left(\frac{\sqrt{m}\tilde{z}_1}{H}\right) \right] \right\}. \quad (47)$$

Fig. 6 shows a plot of $(\overline{\tilde{c}(\tilde{z}=0,\tilde{t})}^{\tilde{t}} - \overline{\tilde{c}(\tilde{z}=\tilde{z}_1,\tilde{t})}^{\tilde{t}})/c_0$ versus $H/\tilde{z}_1 = 1/z_1$ for several values of α. This shows that in most cases, H can be determined accurately and uniquely. However, when $H \gg \tilde{z}_1$ (i.e. when $1/z_1 \gg 1$), the contours of H are flat, indicating that in this case it is difficult to determine H precisely. This imprecision occurs because the altitude z_1 doesn't extend high enough to adequately probe the vertical change in the CO_2 profile. Furthermore, when $H \approx \tilde{z}_1$ (i.e. when $1/z_1 \approx 1$), then two solutions are possible: one with the minimum in $\overline{c(z,t)}^t$ located at an altitude less than z_1, and one with the minimum in $\overline{c(z,t)}^t$ located higher than z_1. This behaviour is graphically illustrated in the upper right-hand panel of Fig. 4, which shows that $\overline{c(z,t)}^t$ equals a given small negative value at two different altitudes. If these problems arise, then one must measure CO_2 at a different or additional altitude.

Once $H = \sqrt{2K_0/\omega_0}$ is determined, then since the angular frequency of a day, ω_0, is a known constant, the eddy diffusivity K_0 is known. Then the amplitude of the surface flux F_0 can be inferred from the definition $c_0 = F_0/(2\,\omega_0\,K_0)^{1/2}$.

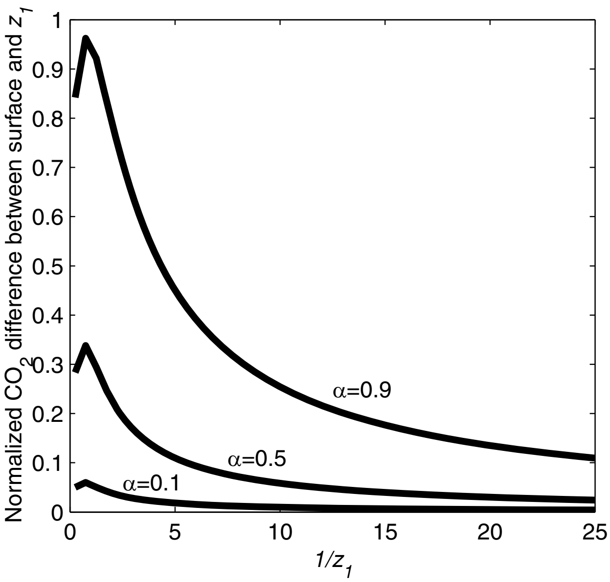

Fig. 6. Along the vertical axis is plotted the left-hand side of eq. (47), that is, the difference in CO_2 mixing ratio between the ground and a height $\tilde{z}_1$ aloft, normalized by the CO_2 scale, c_0. Along the horizontal axis is plotted $H/\tilde{z}_1 = 1/z_1$, where H is the scale height of CO_2. Three curves are plotted for three different values of α. For most values of normalized CO_2 difference, H is straightforward to retrieve. However, when H is small, multiple solutions exist. Furthermore, when H is much larger than the measurement altitude, $\tilde{z}_1$, then H cannot be retrieved precisely.

If no measurements of CO_2 are available aloft, then in order to infer F_0, one may use an estimate of K_0 from another source, if one is available.

(iv) Given the surface average mixing ratio, $\overline{\tilde{c}(\tilde{z}=0,\tilde{t})}^{\tilde{t}}$, [and $\tilde{S}(\tilde{t})$, α, and c_0], calculate the reference CO_2 mixing ratio, $\tilde{c}_{\text{ref}}$:

$$\overline{\tilde{c}(\tilde{z}=0,\tilde{t})}^{\tilde{t}} = \tilde{c}_{\text{ref}} + \frac{1}{\omega_0}\int_{-\infty}^{\tilde{t}} \tilde{S}(\tilde{t}')d\tilde{t}' + c_0\frac{2}{\alpha}\sum_{m=1}^{\infty}\frac{[J_m(m\alpha)]^2}{\sqrt{m}}. \tag{48}$$

To obtain this, we have combined eqs (8), (25) and (34). Because $\tilde{S}$ is regarded as known in this problem, only the constant $\tilde{c}_{\text{ref}}$ needs to be determined.

Because the strength of the rectifier in this simplified model depends only on a single parameter, α, the inverse calculation requires that we numerical calculate only two roots, one for eq. (45) and one for eq. (47). Each of these equations needs to be solved for a single variable alone. Finding such single-variable roots typically requires little computational time.

7. Conclusions

We have constructed an idealized model of the vertical CO_2 rectifier effect. In the model, transport of CO_2 is represented by a prescribed eddy diffusivity. The key feature of the model is that the eddy diffusivity varies diurnally. During the day, the eddy diffusivity is larger, representing daytime convective vertical transport; during the night, the eddy diffusivity is smaller, representing nighttime stable stratification and weak vertical transport.

Prior authors have noted that the diurnal rectifier effect arises from non-zero covariance of CO_2 surface flux and CO_2 vertical transport (e.g. Denning et al., 1996b). We prove a somewhat similar relationship in Section 3. Specifically, we show that in our model, the time-averaged profile of CO_2 mixing ratio is uniform in the vertical (as typical for an unrectified solution) if and only if there is zero covariance in time between the perturbation eddy diffusivity and vertical gradient of CO_2 mixing ratio. Relatedly, we also show that the existence of the rectifier effect in our model depends on whether the vertical transport behaves the same during day as during night (see Section 4). Specifically, we prove that the diurnal cycle of CO_2 mixing ratio in our model is asymmetric in time (as typical for a rectified case) if and only if the eddy diffusivity is not [periodic with a period of one-half day]. This proof relies on the fact that our model's CO_2 surface flux has day–night antisymmetry.

The point of these proofs is isolate the essential ingredients needed in an eddy diffusivity model to yield a rectified or unrectified profile. We hope that in the future this intuition will be useful in revealing rectifier-like effects for other tracers, such as those already proposed for O_2 (Stephens et al., 1998; Gruber et al., 2001).

Our rectifier model can be solved analytically in terms of an infinite series solution (27). In non-dimensionalized form, the model equations and solutions depend on a single parameter, α. This rectifier parameter represents the degree of day–night difference in the magnitude of eddy diffusivity (see eq. 24). When $\alpha = 0$, the eddy diffusivity is constant and the rectifier effect vanishes. When α approaches 1, the eddy diffusivity is much stronger during the day than at night, and the rectifier effect is pronounced.

The rectifier parameter α can be simply but quantitatively related to the surplus surface CO_2 mixing ratio associated with the rectifier effect. We find a relationship in the form of an exact infinite series (34), a Taylor series approximation valid for small α (35) and a Chebyshev polynomial approximation (37) valid over the range $0 < \alpha \leq 0.95$. In this way, the single parameter that represents diurnal variations in turbulent transport, namely α, can be directly linked to the strength of the rectifier effect.

Because the single-parameter solution (27) is simple, it facilitates inverse computations. As an example, we discuss the construction of a complete, 1-D, time-evolving solution for CO_2, given a measurement of the time series of CO_2 mixing ratio at a location at the surface and at a single higher altitude. The solution includes the amplitude of the diurnal surface flux of CO_2. To determine the complete model solution, we need merely to numerically compute the root of each of two equations. Since each of these equations has only one unknown, the desired roots can be calculated inexpensively.

In addition to facilitating inverse computations, the model illustrates conceptual points that may apply to more sophisticated inverse methods. For instance, the equations reveal that this particular diurnal rectifier inversion problem has some potential pitfalls. Specifically, inferring the depth of vertical transport requires measurement at two or more altitudes. Therefore, a surface measurement alone is insufficient if vertical transport is unknown—additional measurements are required, from a tower for instance. This is because surface CO_2 time series are fundamentally ambiguous in this 1-D setting: the same time series may arise from strong surface flux and transport, or weak flux and transport. Furthermore, when CO_2 is measured at two and only two altitudes, there may remain further ambiguities. If the measurement altitude aloft is too low, the inverse estimate may be imprecise when CO_2 mixing is deep. When the altitude of measurement is about the same as the depth over which CO_2 mixes, then the solution may be non-unique. We speculate that measurements at multiple, strategically chosen altitudes would resolve these problems. The above considerations may prove useful in design of field measurements of CO_2 mixing ratio.

In a future application, the prescribed diurnal eddy diffusivity (24) and surface flux (6) could be imposed for CO_2 in each grid column of an atmospheric model with three spatial dimensions. The strength of the rectifier effect could then be specified by setting the parameter α. By performing sensitivity studies with different values of α, one could explore how the rectifier effect combines with 3-D transport to produce large-scale patterns of CO_2 mixing ratio. If the mixing ratio of CO_2 at a particular surface point in the atmospheric model differs from the value expected by 1-D theory (i.e. eq. 27), then it indicates that 3-D transport has a significant effect at that point.

8. Acknowledgments

The authors thank Chuixiang Yi and an anonymous reviewer for numerous comments that improved the manuscript. VEL is grateful for financial support from a Research Growth Initiative Award from the University of Wisconsin – Milwaukee.

References

Abramowitz, M. and Stegun, I. A. 1965. *Handbook of Mathematical Functions*. Dover Publications, New York, 1046 pp.

Arfken, G. 1985. *Mathematical Methods for Physicists*. 3rd Edition, Academic Press, San Diego, CA, USA, 985 pp.

Baker, I., Denning, A. S., Hanan, N., Prihodko, L., Uliasz, M. and co-authors. 2003. Simulated and observed fluxes of sensible and latent heat and CO_2 at the WLEF-TV tower using SiB2.5. *Global Change Biol.* **9**, 1262–1277.

Bakwin, P. S., Davis, K. J., Yi, C., Wofsy, S. C., Munger, J. W. and co-authors. 2004. Regional carbon dioxide fluxes from mixing ratio data. *Tellus* **56B**, 301–311.

Boas, M. L. 1983. *Mathematical Methods in the Physical Sciences*. 2nd Edition, John Wiley and Sons, New York, 793 pp.

Braswell, B. H., Sacks, W. J., Linder, E. and Schimel, D. S. 2005. Estimating diurnal to annual ecosystem parameters by synthesis of a carbon flux model with eddy covariance net ecosystem exchange observations. *Global Change Biol.*, **11**, 335–355.

Chen, B., Chen, J. M., Liu, J., Chan, D., Higuchi, K. and co-authors. 2004. A vertical diffusion scheme to estimate the atmospheric rectifier effect. *J. Geophys. Res.* **109** D04306. doi:10.1029/2003JD003925.

Davis, K. J., Bakwin, P. S., Yi, C., Berger, B. W., Zhao, C. and co-authors. 2003. The annual cycles of CO_2 and H_2O exchange over a northern mixed forest as observed from a very tall tower. *Global Change Biol.* **9**, 1278–1293.

Denning, A. S., Fung, I. Y. and Randall, D. A. 1995. Latitudinal gradient of atmospheric CO_2 due to seasonal exchange with land biota. *Nature* **376**, 240–243.

Denning, A. S., Collatz, G. J., Zhang, C., Randall, D. A., Berry, J. A. and co-authors. 1996a. Simulations of terrestrial carbon metabolism and atmospheric CO_2 in a general circulation model. Part 1: surface carbon fluxes. *Tellus* **48B**, 521–542.

Denning, A. S., Randall, D. A., Collatz, G. J. and Sellers, P. J. 1996b. Simulations of terrestrial carbon metabolism and atmospheric CO_2 in a general circulation model. Part 2: simulated CO_2 concentrations. *Tellus* **48B**, 521–542.

Denning, A. S., Takahashi, T. and Friedlingstein, P. 1999. Can a strong atmospheric CO_2 rectifier effect be reconciled with a ''reasonable" carbon budget? *Tellus* **51B**, 249–253.

Gradshteyn, I. S. and Ryzhik, I. M. 1980. *Table of Integrals, Series, and Products*. Academic Press, San Diego, CA, USA, 1160 pp.

Gruber, N., Gloor, M., Fan, S.-M. and Sarmiento, J. L. 2001. Air-sea flux of oxygen estimated from bulk data: implications for the marine and atmospheric oxygen cycles. *Global Biogeochem. Cycles* **15**, 783–803.

Gurney, K. R., Law, R. M., Denning, A. S., Rayner, P. J., Baker, D. and co-authors. 2002. Towards robust regional estimates of CO_2 sources and sinks using atmospheric transport models. *Nature* **415**, 626–630.

Gurney, K. R., Law, R. M., Denning, A. S., Rayner, P. J., Baker, D. and co-authors. 2003. TransCom 3 CO_2 inversion intercomparison: 1. Annual mean control results and sensitivity to transport and prior flux information. *Tellus* **55B**, 555–579.

Heimann, M., Keeling, C. D. and Fung, I. Y. 1986. Simulating the atmospheric carbon dioxide distribution with a three-dimensional tracer model. In: *The Changing Carbon Cycle: A Global Analysis* (eds J. R. Trabalka and D. E. Reichle), Springer-Verlag, New York, 16–49.

Keeling, C. D., Piper, S. C. and Heimann, M. 1989. A three-dimensional model of atmospheric CO_2 transport based on observed winds: 4. Mean annual gradients and interannual variations. In: *Aspects of Climate Variability in the Pacific and the Western Americas* (ed. D. H. Peterson), Geophys. Monogr. 55, Am. Geophys. Union, 305–363.

Law, R. M., Rayner, P. J. and Wang, Y. P. 2004. Inversion of diurnally varying synthetic CO_2: network optimization for an Australian test case. *Global Biogeochem. Cycles* **18**, GB1044, doi:10.1029/2003GB002136.

Peylin, P., Rayner, P. J., Bousquet, P., Carouge, C., Hourdin, F. and co-authors. 2005. Daily CO_2 flux estimates over Europe from continuous atmospheric measurements: 1, inverse methodology. *Atmos. Chem. Phys. Discuss.* **5**, 1647–1678.

Stephens, B. B., Keeling, R. F., Heimann, M., Six, K. D., Murnane, R. and co-authors. 1998. Testing global ocean carbon cycle models using measurements of atmospheric O_2 and CO_2 concentration. *Global Biogeochem. Cycles* **12**, 213–230.

Stephens, B. B., Wofsy, S. C., Keeling, R. F., Tans, P. P. and Potosnak, M. J. 2000. The CO_2 budget and rectification airborne study: strategies for measuring rectifiers and regional fluxes. In: *Inverse Methods in Global Biogeochemical Cycles* (eds P. Kasibhatla. co-editors), volume 114 of *Geophys. Monogr. Ser.* American Geophysical Union, Washington, DC, 311–324.

Stephens, B. B., Gurney, K. R., Tans, P. P., Sweeney, C., Peters, W. and co-authors. 2007. Weak northern and strong tropical land carbon uptake from vertical profiles of atmospheric CO_2. *Science* **316**, 1732–1735.

Stull, R. B. 1988. *An Introduction to Boundary Layer Meteorology*. Kluwer Academic Publishers, Dordrecht, Netherlands. 666 pp.

Yi, C., Davis, K. J., Bakwin, P. S., Berger, B. W. and Marr, L. C. 2000. Influence of advection on measurements of the net ecosystem-atmosphere exchange of CO_2 from a very tall tower. *J. Geophys. Res.* **105**, 9991–9999.

Yi, C., Davis, K. J., Berger, B. W. and Bakwin, P. S. 2001. Long-term observations of the dynamics of the continental planetary boundary layer. *J. Atmos. Sci.* **58**, 1288–1299.

Yi, C., Davis, K. J., Bakwin, P. S., Denning, A. S., Zhang, N. and co-authors. 2004. Oberved covariance between ecosystem carbon exchange and atmospheric boundary layer dynamics at a site in northern Wisconsin. *J. Geophys. Res.* **109**. D08302.doi:10.1029/2003JD004164.